

Accuracy of Tracked 2D Ultrasound during Minimally Invasive Cardiac Surgery

Andrew D. Wiles^{1,3}, Cristian A. Linte^{2,3}, Chris Wedlake³,
John Moore³, and Terry M. Peters^{1,2,3}

¹ Dept. of Medical Biophysics, The University of Western Ontario

² Biomedical Engineering, The University of Western Ontario

³ Imaging Research Laboratories, Robarts Research Institute
London, Ontario, Canada

{awiles,clinte,cwedlake,jmoore,tpeters}@imaging.robarts.ca

Abstract. A 2D ultrasound enhanced virtual reality surgical guidance system has been developed in our laboratory. The system was tested in both the laboratory and the clinic. Recently, we studied the accuracy of two the ultrasound calibration methods with five different ultrasound transducers using a spherical object as the test platform. In this paper, we extend that work to use the superior vena cava and right atrium of a beating heart phantom as the metrological test artefact. The right atrium was imaged using the tracked ultrasound and the expected cross-sectional outline was determined using the intersection of the ultrasound plane and the surface model in the surgical guidance system. The expected and observed outlines are compared. The results show that the ultrasound calibration methods were sufficiently accurate in the spatial domain, but that temporal calibration is required to ensure accuracy throughout a given procedure.

1 Introduction

Traditional intracardiac surgeries are highly invasive procedures. The patient is opened at the sternum, placed on a cardiopulmonary bypass (heart-lung) machine and their heart is arrested so that the therapy can be applied. Risks to the patient include long recovery times, adverse immune response and possible neurological damage. To address these risks, we have developed an ultrasound enhanced virtual reality system whereby the therapy is applied to the beating heart using either (i) a mini-thoracotomy via the Universal Cardiac Introducer[®] (UCI) [1,2] or (ii) via a percutaneous approach. The Atamai Viewer (www.atamai.com), a software package based on the Visualization Toolkit (VTK, www.kitware.org), is the foundation of the virtual reality software enhanced with real-time 2D ultrasound. The ultrasound transducer and surgical tools are tracked using a magnetic tracking system (Aurora[®], NDI, Waterloo, ON, Canada) which, when employed in conjunction with a virtual environment, provides the surgeon with an interactive environment without direct vision.

Here we extend our previous work [3–5] on the evaluation of the performance of such systems. The system was tested for (i) targeting a static point source [3],

(ii) the insertion of a mitral valve in an ex-vivo porcine heart [4], and (iii) the identification of objects of point source and larger sized objects [5]. Here, we extend the work from [5] which used an approach similar to [6] except that both trueness and precision were assessed for the point source testing. Also, the 3D reconstruction used in [6] was ignored in favour of studying the difference between the outlines of the cross-section of a spherical object (table-tennis ball) appearing in the 2D ultrasound image, and the predicted outline of the spherical object based on the *a priori* model. In this paper, the spherical object is replaced with the inner surface of the superior vena cava and upper portion of the right atrium of a beating heart phantom (Chamberlain Group, Great Barrington, MA, USA) under static conditions. A geometrical model of the right atrium was created from a CT scan and the actual chamber was imaged using the ultrasound enhanced virtual reality surgical guidance system. The expected outline, computed using the intersection of the ultrasound plane and the geometrical model, was compared to the observed outline in the ultrasound image. The experiment was performed using two different ultrasound calibration methods (Z-bar [7] and phantomless [8]), and five different ultrasound transducers. We report on the agreement between the observed images and the expected outlines and provide a discussion on the level of performance observed.

2 Methods

The goal of this experiment is to test how well the tracked ultrasound image agrees with a virtual model of a static object⁴. In order to provide clinical context to the experiment, we chose to use a beating heart phantom as the metrological test platform. Several fiducial markers, whose positions were determined by identifying them with a tracked 3.2mm spherical tool tip, were placed on the heart surface and the mounting base for registration purposes (see Fig. 1).

A static CT scan of the heart phantom was obtained and the CT scan was segmented using the Vascular Modelling Toolkit (VMTK⁵) and ITK Snap. Two surface meshes were segmented from the CT volume for (i) the epicardial surface and (ii) the superior vena cava along with the upper portion of the right atrium. The surface model of the superior vena cava and the right atrium is provided in Fig. 1.

The beating heart phantom was placed in a 7% glycerol solution bath so that the various ultrasound transducers operated at the appropriate speed of sound (1540m/s). The images and surface models were loaded into the surgical guidance system and the models were registered with the phantom heart by digitizing the fiducial markers using the magnetic tracking system.

A 6 DoF magnetic tracking sensor was placed on each ultrasound transducer. The transducer was spatially calibrated using first the Z-Bar [7] and then the phantomless [8] methods. Once calibrated, the ultrasound image was tracked and displayed in the surgical guidance system (see [1] for details). The cross-sectional

⁴ Future work includes performing a dynamic test with a temporal calibration.

⁵ VMTK: <http://villacamozi.marionegri.it/~luca/vmtk/doku.php>

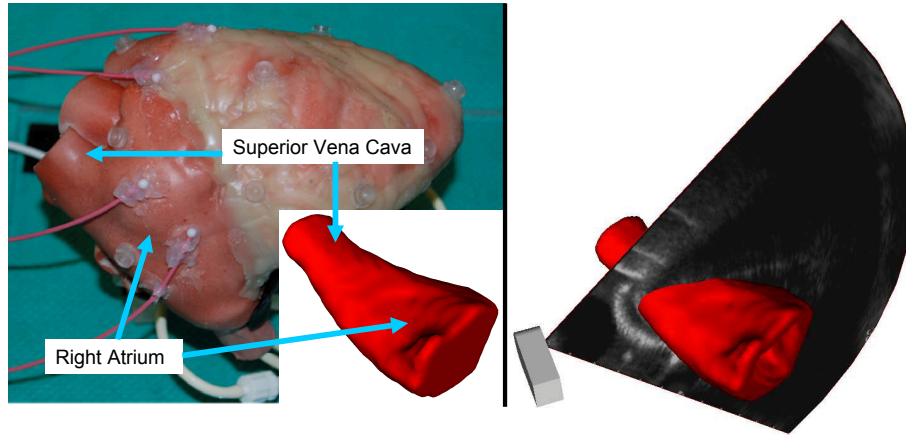


Fig. 1: Left, beating heart phantom and segmented surface of the superior vena cava and right atrium. Right, segmented surface being imaged by the Adult TEE where the expected outline occurs at the intersection of the ultrasound plane and segmented surface. Clear objects on the heart surface are fiducial markers. Pink flexcords with teflon balls on the tip are metrological devices for another study.

outline of superior vena cava and right atrium in the AP/LR plane were imaged at several points along the surface model. The expected outline was determined from the intersection of the infinite plane formed by the ultrasound fan and the surface model of the vena cava and right atrium using the `vtkCutter` class from VTK (see Fig. 1). The observed outline was marked on the ultrasound image itself. A sample ultrasound image using the adult transesophageal probe from Philips is provided in Fig. 2 where the expected and observed outlines are marked in green and yellow, respectively.

The points that define the outline form an irregular polygon. The centroid and area of the expected and observed polygons are computed by respectively averaging the center of mass and areas of a collection of triangles that were formed by the polygonal vertices. The expected and observed centroid positions and areas are compared and summarized in section 3.

3 Results

In all, two ultrasound calibration methods (Z-Bar [7] and phantomless [8]) were tested along with five different ultrasound transducers: (i) Aloka neuro echo transducer (N), (ii) Philips adult transesophageal echo transducer (AT), (iii) Philips pediatric transesophageal echo transducer (PT), (iv) Sequoia AcuNav intracardiac echo transducer (IC), (v) Aloka laparoscopic echo transducer (L). In all, only 9 tests were performed because the Z-bar phantom used at our laboratory is too large for the laparoscopic probe's field of view.

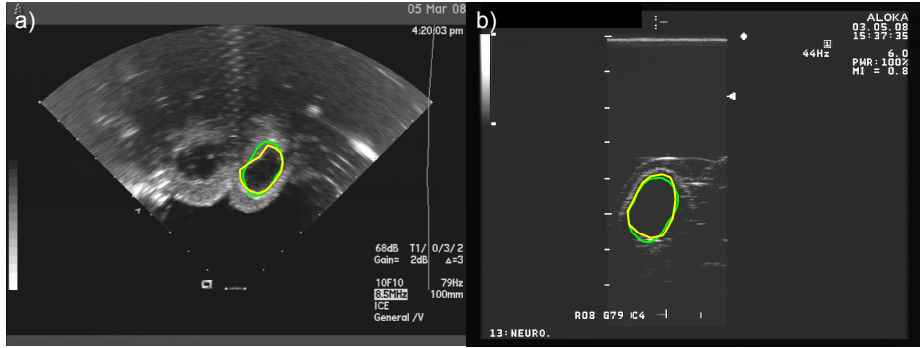


Fig. 2: Sample image of the right atrium with the expected (green) and observed (yellow) outlines for the a) intracardiac probe and b) laparoscopic probe.

For each image of the right atrium surface model, the outline was marked with up to 16 points in the ultrasound image to form an irregular polygon. The centroid and areas of the expected and observed outlines were computed. The centroid distance error (d_{err}) is found by taking the magnitude of the difference between the observed outline centroid (\mathbf{p}_o) and the expected outline centroid (\mathbf{p}_e) given by $\|\mathbf{p}_o - \mathbf{p}_e\|$. The area percent difference was computed using the expected area as the reference such that $\%_{diff} = 100 \cdot (A_o - A_e) / A_e$. The centroid distance error RMS and the area percent difference mean and standard deviation are summarized in Table 1. Fig. 3 provides two plots, one for Z-bar calibrations and one for phantomless calibrations, which show the distribution of the centroid error on the image plane. Fig. 4 shows the distribution of the centroid distance error using a box plot format. The box plots are a better method to examine these than the statistics provided in Table 1 since the distributions are one-sided resulting in a non-Gaussian distribution.

Table 1: Summary results for the centroid error and area percent difference.

Transducer	Z-Bar Calibration		Phantomless Calibration	
	Centroid RMS	Area % Diff	Centroid RMS	Area % Diff
N	1.82	$8.6 \pm 12.3\%$	2.18	$3.1 \pm 12.1\%$
AT	5.68	$16.1 \pm 11.4\%$	2.64	$-4.7 \pm 11.5\%$
PT	3.12	$-26.3 \pm 10.3\%$	4.38	$-12.6 \pm 24.0\%$
IC	1.07	$-17.14 \pm 10.0\%$	2.78	$-18.0 \pm 8.7\%$
L	-	-	1.79	$13.8 \pm 7.4\%$

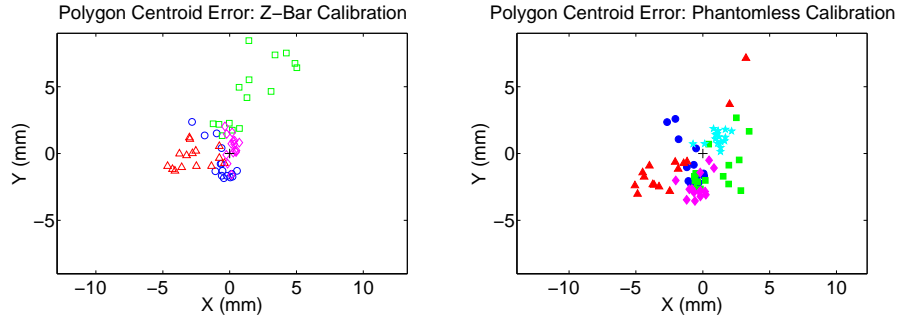


Fig. 3: Centroid Error. Centroid position error for observed and expected outlines are plotted on the image plane for the neuro transducer (\circ, \bullet), adult TEE (\square, \blacksquare), pediatric TEE ($\triangle, \blacktriangle$), ICE (\diamond, \blacklozenge) and laparoscopic transducer (\star). Hollow symbols: Z-bar. Filled symbols: Phantomless. Origin is marked with +.

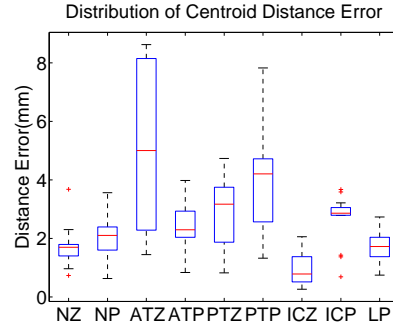


Fig. 4: Box plots showing the distribution of the centroid error for each test case.

4 Discussion

In our previous work [5], we noticed a significant difference in the transformations computed using the two different calibration methods. We attributed this to the need for the phantomless calibration tool to be held at multiple orientations relative to the ultrasound plane. For the experiments described here, we were able to set up the calibration such that the tracked calibration probe could be placed in a wider range of orientations. Therefore, the calibration matrices obtained from each calibration method were more similar, although the translations still differ by distances up to 3-4mm. Further investigation on how to optimize the two methods to ensure a proper calibration will be continued in the future.

In general, the results in Table 1 show that the two calibration methods perform well for our surgical guidance system. However, the centroid error RMS is quite high for the Adult TEE using the Z-Bar calibration as it approaches 6mm. The box plot in Fig. 4 shows the error ranging from less than 2mm to

more than 8mm. After examining some of the results we noticed a significant discrepancy in the data where some of the outlines matched poorly (Fig. 5a) and some them matched quite well (Fig. 5b). The Adult TEE with the Z-Bar was the first completed test case and some difficulty was experienced in holding the transducer steady, resulting in the ultrasound image moving during the data collection. This experiment was designed with the expectation that the data would be collected under pseudo-static conditions, i.e., the probe would be held steady at each collection. Hence, no temporal calibration was completed and the ultrasound video feed and the tracking system were not synchronized. Therefore, any movement of the transducer at the time of collection would result in an additional error such as the one seen in Fig. 5a. As the remaining test cases were completed, the user operating the ultrasound transducer became better at maintaining the pseudo-static requirements and the results improved. It is expected that our future work in this area will include a temporal calibration, particularly as we venture into experiments using a dynamic environment.

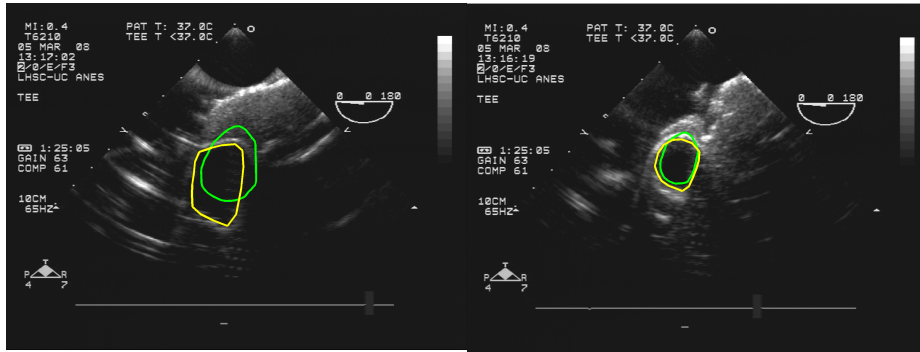


Fig. 5: Two examples for the Adult TEE probe using the Z-Bar calibration. In a) a translation between the expected and observed is seen but in b) the two are aligned quite well. The discrepancy is caused by the lack of a temporal registration and movement of the sensor in a).

We also noted some discrepancies in the surface model obtained from the CT and the actual cavity shown on the ultrasound image. Fig. 6a shows an image obtained where the expected outline is much smaller in area than observed. The enlarged view in the inset shows that there is no indication of any sort that the rear portion of the chamber exists in the ultrasound image. This is not due to the errors introduced by the lack of a temporal calibration, but is caused by the inability of the neuro ultrasound transducer to image the thin wall at the junction of the right atrium and pulmonary artery.

As shown in Fig. 6b, the outline observed using the pediatric probe was often smaller than expected. The point spread function in the transducer causes the boundaries of the right atrium to be blurred such that there is no clear indication as to where the boundary exists. The enlarged inset shows the level of blur

for this transducer and also explains why the area of the polygons was consistently smaller than expected. A similar effect was observed with the intracardiac transducer.

These discrepancies are a very good indication of why the ultrasound enhanced VR system is needed for accurate intracardiac surgery. In each of these cases the VR model provides an additional level of context for the actual shape of the vessel or chamber. This information would not be available in a procedure where only a 2D or 3D ultrasound image was used for guidance.



Fig. 6: Examples of errors caused by the ultrasound image for a) neuro probe and b) the pediatric TEE probe. The insets provide enlarged views of the right atrium without the expected or observed outlines. In a) the expected outline is much further away from the transducer than the observed outline. The image provided by the pediatric TEE in b) shows how blurred the surface edges become due to the point spread function of the ultrasound transducer.

In the results presented here the errors are based on a single ultrasound calibration for each test case. It would be beneficial if the uncertainty of the calibration could be modelled statistically whereby the calibration transformation matrix would have a 6×6 covariance matrix for the independent transformation parameters which would in turn provide an uncertainty model for the expected outlines. One method to determine the calibration uncertainty involves repeating the calibration 100 or 1000 times to generate a statistical sampling. However, this method is a daunting task where the time it takes to collect and mark the calibration images is significant. But, since both calibration methods fundamentally rely on a point-based registration, the uncertainty of the ultrasound coordinate frame can be estimated using target registration error (TRE) models [9,10]. The difficulty with this method is that determining accurate statistical models of the fiducial localizer error (FLE) is complicated. If we could estimate the FLE for each homologous point used in the registration, then the estimation of the calibration uncertainty would be trivial.

5 Conclusions and Future Work

It is clear that the two calibration methods are sufficient for calibrating the tracked ultrasound images, although it is critical that temporal calibration is also completed. Future work will include repeating this study under dynamic conditions and developing a statistical model that describes the uncertainty of a given ultrasound calibration.

Acknowledgements

The authors would like to thank Jacques Milner and Dr. Usaf Aladl at the Robarts Research Institute for their help in the image segmentation. This work was supported by CIHR, NSERC, ORDCCF, CFI, UWO and NDI.

References

1. Linte, C.A., Moore, J., Wiles, A.D., Wedlake, C., Peters, T.M.: Virtual reality-enhanced ultrasound guidance: A novel technique for intracardiac interventions. *Computer Aided Surgery* **13**(2) (March 2008) 82–94
2. Guiraudon, G.M., Jones, D.L., Bainbridge, D., Peters, T.M.: Mitral valve implantation using off-pump closed beating intracardiac surgery: A feasibility study. *Interact Cardiovasc Thorac Surg* **6**(5) (Oct 2007) 603–607
3. Wiles, A.D., Guiraudon, G.M., Moore, J., *et al.*: Navigation accuracy for an intracardiac procedure using ultrasound enhanced virtual reality. In Cleary, K.R., Miga, M.I., eds.: *Medical Imaging 2007: Visualization and Image-Guided Procedures*. Volume 6509., SPIE (2007) 65090W
4. Linte, C., Wiles, A.D., Hill, N., *et al.*: An augmented reality environment for image-guidance of off-pump mitral valve implantation. In Cleary, K.R., Miga, M.I., eds.: *Medical Imaging 2007: Visualization and Image-Guided Procedures*. Volume 6509., SPIE (2007) 65090N
5. Wiles, A.D., Moore, J., Linte, C.A., Wedlake, C., Ahmad, A., Peters, T.M.: Object identification accuracy under ultrasound enhanced virtual reality for minimally invasive cardiac surgery. In Miga, M.I., Cleary, K.R., eds.: *Medical Imaging 2008: Visualization, Image-guided Procedures*. Volume 6918., SPIE (2008) 69180E
6. Rousseau, F., Hellier, P., Letteboer, M.M., Niessen, W.J., Barillot, C.: Quantitative evaluation of three calibration methods for 3-D freehand ultrasound. *IEEE Trans Med Imaging* **25**(11) (Nov. 2006) 1492–1501
7. Gobbi, D.G., Comeau, R.M., Peters, T.M.: Ultrasound probe tracking for real-time ultrasound/MRI overlay and visualization of brain shift. In: *Medical Image Computing and Computer-Assisted Intervention - MICCAI 1999*. Volume LNCS 1679. (1999) 920–927
8. Khamene, A., Sauer, F.: A novel phantom-less spatial and temporal ultrasound calibration method. *MICCAI 2005, 8th International Conference Medical Image Computing and Computer Assisted Intervention* **8**(Pt 2) (2005) 65–72
9. Fitzpatrick, J.M., West, J.B., Maurer, C.R.: Predicting error in rigid-body point-based registration. *IEEE Trans Med Imaging* **17**(5) (Oct 1998) 694–702
10. Wiles, A.D., Likholyot, A., Frantz, D.D., Peters, T.M.: A statistical model for point-based target registration error with anisotropic fiducial localizer error. *IEEE Trans Med Imaging* **27**(3) (March 2008) 378–390